A Correlation Filtering-based Matching Pursuit (CF-MP) for Damage Identification Using Lamb Waves

Article *in* Smart Materials and Structures · October 2006

DOI: 10.1088/0964-1726/15/6/010

4 authors, including:

Fucai Li
Shanghai Jiao Tong University
65 PUBLICATIONS **480** CITATIONS
SEE PROFILE

Guang Meng
Shanghai Jiao Tong University
550 PUBLICATIONS **4,118** CITATIONS
SEE PROFILE

INSTITUTE OF PHYSICS PUBLISHING SMART MATERIALS AND STRUCTURES
Smart Mater. Struct. **15** (2006) 1585–1594 doi:10.1088/0964-1726/15/6/010

A correlation filtering-based matching pursuit (CF-MP) for damage identification using Lamb waves

Fucai Li[1,2], Zhongqing Su[1], Lin Ye[1,3] and Guang Meng[2]

[1] Laboratory of Smart Materials and Structure (LSMS), Centre for Advanced Materials Technology (CAMT), School of Aerospace, Mechanical and Mechatronic Engineering, The University of Sydney, NSW 2006, Australia
[2] State Key Laboratory of Vibration, Shock and Noise, Shanghai Jiao Tong University, 1954 Huashan Road, Shanghai 200030, People's Republic of China

E-mail: ye@aeromech.usyd.edu.au

Received 27 January 2006, in final form 24 July 2006
Published 3 October 2006
Online at stacks.iop.org/SMS/15/1585

Abstract
Time of flight (ToF) plays a key role in positioning structural damage, but the exact determination of ToF in complicated Lamb wave signals is somewhat challenging. A signal processing approach, taking advantage of correlation filtering-based matching pursuit (CF-MP), was developed. In this approach, correlation among wave signals captured from the same structure under different damage statuses was calibrated, which served as an indicator for the occurrence and severity of structural damage. The ToF of a damage-scattered Lamb wave was pinpointed with high precision. With it, the approach was then applied to Lamb wave signals acquired from delaminated carbon-fibre/epoxy (CF/EP) composite beams, and the location and size of the delamination were exactly predicted. Experimental validation indicated that such an approach is able to filter boundary-reflected signal components involved in a complex wave signal, making the wave-based damage identification technique practical for small structures.

(Some figures in this article are in colour only in the electronic version)

1. Introduction

Lamb waves, guided elastic waves in a thin plane, have been examined as a means of establishing novel non-destructive evaluation (NDE) approaches [1–7]. By using the *time of flight* (ToF) (the time lag between the incipient wave and the damage-reflected wave) in the captured signals from one sensor–actuator pair, structural damage can be located [8]. However, the interpretation and understanding of Lamb wave signals is a notoriously complex issue. In particular, compared with a Lamb wave excited by angle-variable ultrasonic probes coupled with an angle-adjustable Perspex wedge, multiple Lamb modes, including symmetric (S_0) and anti-symmetric (A_0) modes, will be generated simultaneously when a piece of piezoelectric element is used as actuator. With a very fast propagation velocity, the incipient wave can be rapidly reflected by the structural boundary, considerably obscuring the damage-scattered components in the signals. This interference is a particularly serious concern in small structures. Exact determination of ToF in Lamb wave signals, and consequent damage evaluation, accordingly becomes challenging.

A variety of pragmatic signal processing and identification approaches have been developed and have contributed to the ascertainment of ToF in Lamb wave signals, best exemplified by time-series analysis [9], fast Fourier transform (FFT) [10–13], time-frequency distribution, including short-time Fourier transform (STFT) [14, 15], Wigner–Ville distribution (WVD) [14, 16], wavelet transform (WT) [14, 15, 17–21], etc. Applying these approaches can exactly pinpoint the time moment of the damage-reflected wave in the signal upon filtering of noisy components of no interest. For example, Valdes

[3] Author to whom any correspondence should be addressed.

and Soutis [22] measured the ToF from Lamb wave signals to locate delamination in composite beams and Kessler *et al* [8] enhanced such an approach by introducing WT analysis. Hou *et al* [23] introduced a scale-averaged wavelet power (SAP)-based technique, to offer more accurate measurement of ToF.

In this study, a signal processing and identification algorithm using correlation filtering-based matching pursuit (CF-MP) was developed for exactly determining the ToF in raw Lamb wave signals and for further quantitative damage assessment. The traditional matching pursuit approach was enhanced by introducing it into the wavelet domain. In this approach, correlation of signals from composite laminates containing delamination with those from intact laminates was calibrated, and through this calibration the singularity in the signals attributable to damage was detected. In particular, such an approach effectively filters boundary-reflected signal components, contributing to the applicability of wave-based damage identification techniques for small structures. For validation, the algorithm was applied to delamination identification, including location and size, in quasi-isotropic carbon-fibre/epoxy (CF/EP) composite beams.

2. Correlation filtering-based matching pursuit (CF-MP)

2.1. Matching pursuit

Matching pursuit (MP) is a signal processing algorithm based on an iterative optimization. It decomposes a time-dependent signal into the summation of a series of linear expression functions and therefore offers a sub-optimal presentation for the whole signal [24, 25]. These functions, selected from a redundant dictionary, are termed '*atoms*'. Normally such a dictionary contains over-complete functions well-fitted to all the features in the signal to be processed. At each iteration, the whole dictionary is searched and an atom that is best adapted to the particular segment of the signal is picked up. If the segment cannot be well matched with any specific function in the dictionary, the segment is further decomposed into finer levels while its information is diluted. Upon matching, the current segment is then subtracted from the original signal, and the pursuit is applied to the rest of the signal, named the *residue* [25]. In particular, if the waveform and frequency of the signal to be processed are known, atoms owning the waveform and frequency with the highest similarity with those of the signal can be easily chosen from the dictionary. In such cases decomposition can be most cost-effectively implemented. Note that in most cases a signal can be only approximately correlated using atoms selected from the dictionary, rather than exactly matched. Although an MP-based approach is nonlinear, it maintains an energy conservation which guarantees its convergence [24]. The MP-based approach can now be found widely in the general fields of noise removal, signal compression, feature extraction, etc.

2.2. MP over the orthogonal wavelet dictionary

In the present study, the MP approach was improved by integrating it with the orthogonal wavelet transform. Fundamentally, when applied with a basic orthogonal wavelet transform function, $\Psi(t)$, a time-dependent wave signal, $f(t)$, is converted into a quadratic expression using dual parameters *scale*, a, and *time*, b [18, 26],

$$W(a,b) = \frac{1}{\sqrt{a}} \int_{-\infty}^{+\infty} f(t) \cdot \bar{\Psi}\left(\frac{t-b}{a}\right) \cdot \mathrm{d}t. \qquad (1)$$

The operation performed by equation (1) is defined as a *continuous wavelet transform* (CWT) and $W(a,b)$ is the *CWT coefficient*. $\bar{\Psi}(t)$ denotes the complex conjugate of $\Psi(t)$. For simplification, equation (1) is executed by calculating the wavelet coefficients only at discretized *scale* and *time* using dyadic variables m and n, namely *discrete wavelet transform* (DWT) analysis:

$$a = a_0^m \qquad \text{and} \qquad b = n a_0^m b_0, \qquad m, n \in Z \qquad (2a)$$

$$\mathrm{DWT}(m,n) = a_0^{-\frac{m}{2}} \int f(t) \cdot \Psi(a_0^{-m} t - n b_0) \cdot \mathrm{d}t \qquad (2b)$$

where a_0 and b_0 are constants determining the sampling intervals along the time and scale axes, respectively. Equation (2) decomposes signals into associated scopes of relatively higher and lower frequencies.

A dictionary over the time-scale domain was established, denoted by Θ, where all the atoms are defined as *matching wavelet atoms* (MWAs). To illustrate the mechanism, a sinusoidal tone-burst signal, denoted by $s(t)$, is examined, which is defined as

$$s(t) = \begin{cases} \sin(2\pi f \cdot t + \theta), & t \in [\tau,\ \tau + W_\mathrm{s}] \\ 0, & \text{else} \end{cases} \qquad (3)$$

where f, θ, τ, W_s are the central frequency, phase, starting time and duration of $s(t)$ respectively. A window function, *Hanning window*, $h(n)$, is introduced to modulate $s(t)$, formulated as [27]

$$h(n) = \frac{1}{2}\left[1 - \cos\left(2\pi \frac{n}{n+1}\right)\right], \quad (n = 0, 1, 2, \ldots, N-1) \qquad (4a)$$

with its Fourier counterpart in the frequency domain

$$H(\omega) = \left\{\frac{1}{2} W_\mathrm{R}(\omega) + \frac{1}{4}\left[W_\mathrm{R}\left(\omega - \frac{2\pi}{N-1}\right) + W_\mathrm{R}\left(\omega + \frac{2\pi}{N-1}\right)\right]\right\} \cdot \mathrm{e}^{-\mathrm{j}\left(\frac{N-1}{2}\right)\omega} \qquad (4b)$$

where W_R is the characteristic function for rectangular waveforms, and N is the length of the *Hanning* window. Figure 1(a) depicts the waveform of the MWA selected and figure 1(b) presents its corresponding spectrum via fast Fourier transform (FFT) analysis.

As mentioned earlier, an atom can be easily determined if the waveform and frequency of the signal to be processed are known. Accordingly, an MWA at time τ, denoted by $\psi_\tau(t)$, for the modulated signal was chosen as

$$\psi_\tau(t) = s(t) * h(n) \qquad (n = 0, 1, 2, \ldots, N-1). \qquad (5)$$

In terms of the principle of digital signal processing (DSP), in the case that only the sinusoidal signal component

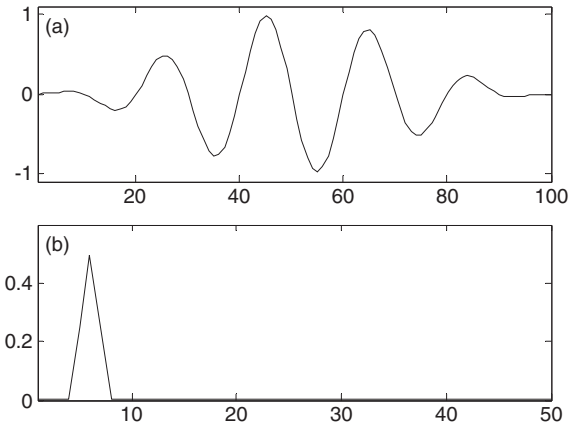

Figure 1. Matching wavelet atom: (a) waveform and (b) FFT spectrum.

(upper part in equation (3)) is considered, $\psi_\tau(t)$ can be further compactly redefined in a discrete form $\psi(k)$ [27]:

$$\psi(k) = 0.5 \cdot \left(1 - \cos\left(2\pi \frac{k}{n-1}\right)\right) \cdot \sin\left(2\pi f \frac{k}{f_s} + \theta\right) \quad (k = 0, 1, 2, \ldots, N-1) \tag{6a}$$

$$N = num \cdot \text{int}\left(\frac{f_s}{f}\right) \tag{6b}$$

where f is the central frequency of $s(t)$; f_s is sampling frequency of the signal under study, hereinafter denoted by $x(t)$; *num* is number of sinusoid cycle; N is the discrete length of the exciting signal. It can be seen that the MWA is a discrete array, whose length is determined by both the central frequency and the cycle number of the MWA as well as the sampling frequency of the raw signal $x(t)$. Meanwhile, the continuous signal, $x(t)$, is also discretized:

$$x(t) = x(m) \qquad (m = 0, 1, 2, \ldots, M-1) \tag{7}$$

where M is the discrete signal length of the signal, and $M > N$. During iteration of the matching pursuit over the wavelet dictionary Θ, the MWA ($\psi(k)$) with the greatest inner product with the segments (with discrete length of N) of $x(m)$ is chosen in the first iteration. Then the inner product is subtracted from the signal. Repeating such an operation on the signal *residue* leads to the matching pursuit for the entire signal over Θ.

2.3. Correlation filtering

It is noted that the wavelet function normally features orthogonality, but the MWA discussed above does not. This may influence the performance of wavelet transform in fast signal decomposition and reconstruction. To address this concern, a correlation-ameliorated MP approach over the wavelet dictionary was introduced.

The correlation, aimed at calibrating the level of similarity between two signals, is defined in terms of the inner product [28]:

$$\langle \psi_\tau(t), x(t) \rangle = \int \psi_\tau(t) \cdot x(t)\, \mathrm{d}t. \tag{8}$$

Since both $x(m)$ and $\psi(k)$ are discrete vectors, their inner product equals the dot product:

$$\langle \psi(k), x_{\tau,N}(m) \rangle = \|\psi\|_2 \|x_{\tau,N}\|_2 \cos\theta \tag{9}$$

where $x_{\tau,N}(m)$ is the signal segment of $x(m)$, with discrete length N and starting time τ, and θ is the inclination between two vectors. In particular, θ goes to zero, namely $\cos\theta = 1$, when two vectors are completely correlated (overlapping in the time domain). A correlation coefficient, K ($K \in R$ and $0 \leqslant K \leqslant 1$), was introduced to quantify the degree of similarity between the time signals, defined as, at time point τ, [29]

$$K_\tau = \cos\theta = \frac{\langle \psi(k), x_{\tau,N}(m) \rangle}{\|\psi(k)\|_2 \left\|x_{\tau,N}(m)\right\|_2}. \tag{10}$$

By shifting the starting time τ of $x(m)$, a series of correlation coefficients, K_τ at different times of pursuit, were obtained, each of which denotes one pursuit status. The degree of similarity between the segment of signal at time τ and the MWA is proportional to K_τ. Such a procedure is termed the correlation filtering-based matching pursuit (CF-MP) [29]. In a CF-MP, a higher value of the correlation coefficient denotes a higher matching pursuit. It can be seen that the shifting step $\Delta\tau$ is of vital importance. Normally a very small $\Delta\tau$ can guarantee excellent matching precision, which is, however, fairly CPU- and memory-intensive. With high-capability computational devices, such concerns are ameliorated. In the present study, the step was set as the least possible, i.e. one sampling point. Furthermore, a threshold was pre-set and the signal was then redefined by retaining in the signal only those segments with a higher K value than the threshold, while removing segments with a coefficient below the threshold. Such an approach is termed correlation filtering.

3. CF-MP-based Lamb wave signal processing

The CF-MP over the wavelet dictionary developed was applied to captured Lamb wave signals in the study. Following the signal defined by equations (3) and (4), *Hanning* function-modulated 5-cycle sinusoidal tone-bursts were used to excite a Lamb wave in a CF/EP composite beam, acquired by a surface-mounted piezoelectric actuator-sensor pair, displayed in figure 2(a). The central frequency of the excited Lamb wave, f, was 100 kHz and the sampling frequency, f_s, was 2.048 MHz. The first wave packet is the fundamental symmetric mode, S_0, in terms of its propagation velocity, referring to the magnified part in figure 2(b). The second packet in the signal is the boundary-reflected S_0, denoted by $S_{0\text{ref}}$.

An MWA in a *Hanning*-windowed sinusoidal waveform was chosen as $\psi(t)$, as in figure 1(a). Shifting the MWA at a step of one sampling point along the time axis, the correlation coefficient, K_τ, at all sampling moments was calculated in terms of equation (10). Its trace is displayed in figure 2(c), with a magnified segment in figure 2(d). Because both the excited Lamb wave signal and the WMA consist of a series of modulated sinusoids, the inclination θ in equation (10) varies following

$$\left[\ldots, -2\pi, \ldots, -\tfrac{3}{2}\pi, \ldots, -\pi, \ldots, -\tfrac{1}{2}\pi, \ldots, 0, \ldots \tfrac{1}{2}\pi, \ldots, \pi, \ldots, \tfrac{3}{2}\pi, \ldots, 2\pi, \ldots\right].$$

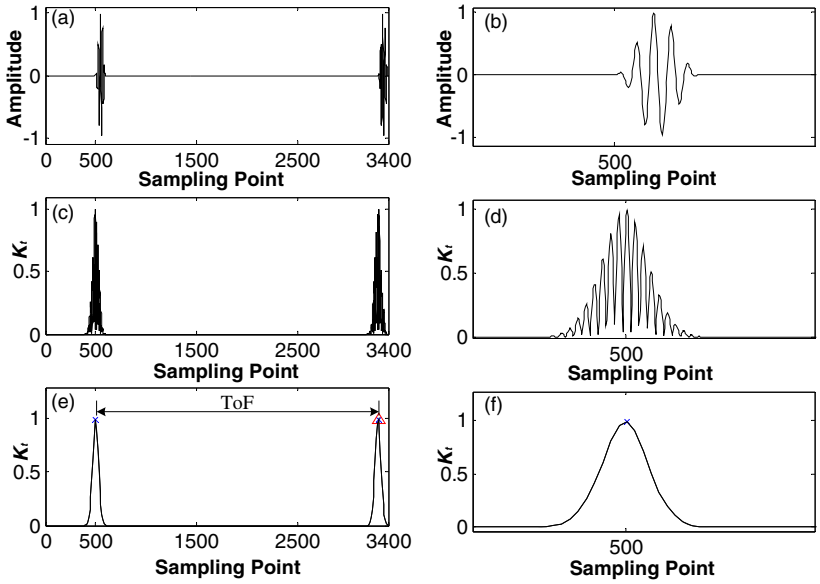

Figure 2. Lamb wave signal from a laminated composite beam without delamination: (a) raw signal; (b) magnified segment of (a); (c) correlation coefficient curve of (a); (d) magnified segment of (c); (e) envelope curve of (c); (f) magnified segment of (e).

Table 1. Characteristic data of CF-MP-processed Lamb wave signal.

	Position of characteristic points (sampling point)	Position of characteristic points (time (ms))	K_τ
Peaks of matching results	481	0.234	0.814 22
	491	0.239	0.961 35
	501	0.244	0.995 21
	511	0.249	0.901 85
	521	0.254	0.717 34
	3241	1.582	0.814 22
	3251	1.587	0.961 35
	3261	1.592	0.995 21
	3271	1.597	0.901 85
	3281	1.602	0.717 34
Peaks of envelope curve of matching results	501	0.244	0.995 21
	3261	1.592	0.995 21

As a result, K_τ oscillates between -1 and 1. θ reaches a peak value at sampling points of $[\ldots -2\pi, -\pi, 0, \pi, 2\pi, \ldots]$, corresponding to the peaks of K_τ, respectively. The first ten peaks of K_τ are listed in table 1. In particular, the correlation coefficient climaxes at the 501st and 3261st sampling points, respectively. Since the best match occurs only at time point τ where θ is equal or very near to zero, for an explicit appearance of the correlation coefficient curve, the envelope curve of K_τ was obtained, and it is exhibited in figure 2(e) with a magnified part in figure 2(f). With only two peaks, respectively at signal packet peaks, the time of flight (ToF) can be concisely calculated from figure 2(f).

4. Evaluation and discussion

4.1. Delamination location

An eight-ply $[45/-45/0/90]_s$ quasi-isotropic carbon fibre/epoxy (CF/EP) composite cantilever beam, measuring 400 mm × 20 mm × 1.275 mm, was evaluated to assess delamination in it, schematically shown in figure 3. One piezoelectric (PZT) actuator–sensor pair was surface-bonded on the beam, and the Lamb waves were generated and collected through it. A through-the-width delamination was introduced between the third and fourth laminate (counting downwards from the upper beam surface) with axis-span a, interlaminar position d, distance L from its right tip to the right beam end (L' from its left tip to the sensor). Modelling techniques previously developed for delamination in terms of contact surface algorithm [30], piezoelectric actuator and sensor [31], and CF/EP composite laminate using effective elastic properties [32] were employed. The beam was finely meshed using eight-note 3D brick elements with eight layers of elements in the beam thickness. CF/EP (T650/F584; Hexcel Co., 2001) was considered, with elastic properties as detailed in table 2. The dynamic simulation was conducted using ABAQUS/EXPLICIT®.

The Lamb wave signal excited by the PZT actuator was 5-cycle sinusoid tone-bursts windowed by the *Hanning* function at a central frequency of 0.1 MHz. The Lamb wave

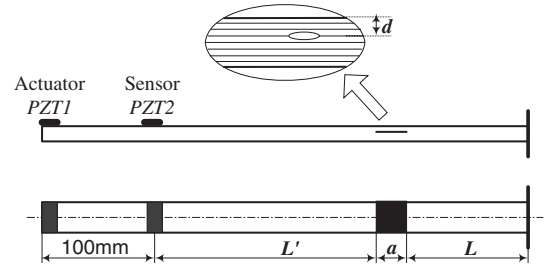

Figure 3. A composite beam containing delamination.

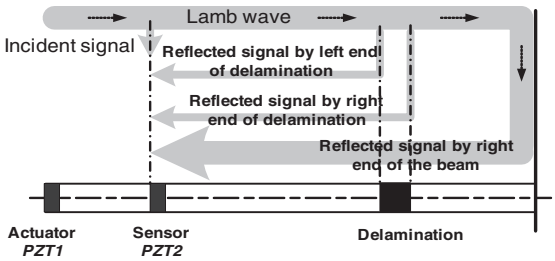

Figure 4. Schematic illustration of propagation paths of Lamb waves in delaminated beam.

Table 2. Technical parameters of CF/EP (T650/F584) composites.

Fibre product name	Matrix product name	Fibre volume (%)	Matrix volume (%)	Laminate density (kg m^{-3})
T650/35-12K	F584	56	44	1528

signals captured by the sensor were then filtered using CF-MP. Since the waveform and frequency of the signal were known, only one MWA with the same waveform over the wavelet function dictionary Θ was chosen. The propagation path of the Lamb wave in the beam is schematically depicted in figure 4, where PZT2 senses the incident wave first (the first wave packet in the captured signal), followed by the signals reflected by both tips of the delamination.

Using the composite beam in figure 3, the CF-MP-processed envelope curves of the delamination-free beam (benchmark) and another four delaminated beams with arbitrarily chosen delamination parameters are displayed in figure 5. For the benchmark signal, R_{pas} in figure 5(a) is the pursuit region of the incident Lamb wave, and R_{ref} is the pursuit region of the reflected incident wave from the right beam end. Compared with the benchmark signal, delamination-induced reflection, including the signals from left and right tips, can be clearly observed in figures 5(b)–(e) for four cases. R_{diff} in figures 5(b)–(e) is the region in which the CF-MP-processed envelope curves of the benchmark and object signal differ greatly, and $P_{\mathrm{S0Dela\ L}}$ and $P_{\mathrm{S0Dela\ R}}$ are the starting positions of the Lamb wave signal reflected from the left and right tips of the delamination in the envelope curve, respectively.

The starting positions (in the time domain) of the incident Lamb wave and of reflected waves from the left and right tips of the delamination in the envelope curve are defined as t_{S0}, $t_{\mathrm{S0Dela\ L}}$ and $t_{\mathrm{S0Dela\ R}}$, respectively. Their corresponding ToF

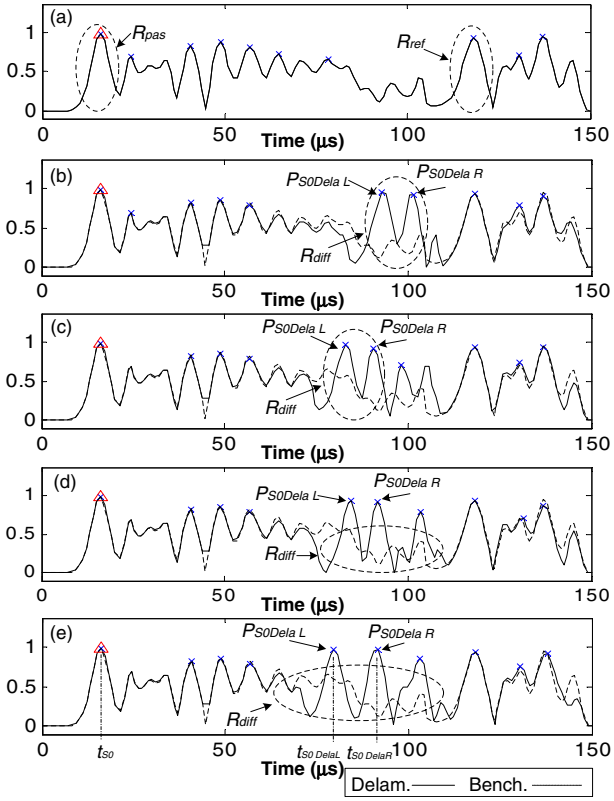

Figure 5. Envelope curves from CF-MP processing for (a) delamination-free beam (benchmark); (b) delaminated beam I ($a = 25$ mm, $L = 50$ mm, $L' = 225$ mm, between the first and second layers); (c) delaminated beam II ($a = 25$ mm, $L = 80$ mm, $L' = 195$ mm, between the third and fourth layers); (d) delaminated beam III ($a = 22$ mm, $L = 80$ mm, $L' = 200$ mm, between the first and second layers); (e) delaminated beam IV ($a = 35$ mm, $L = 80$ mm, $L' = 185$ mm, between the first and second layers).

relative to the sensor can be calculated; and the location of delamination relative to the sensor's location is calculated by (referring to figure 4)

$$L' = \frac{(t_{\mathrm{S0Dela\ L}} - t_{\mathrm{S0}}) \cdot V_{\mathrm{S0}}}{2 \cdot f_{\mathrm{s}}} \tag{11}$$

where L' is the distance between the left tip of the delamination and the centre of PZT2, V_{S0} is the wave propagation velocity of the S_0 mode, and f_{s} is the sampling frequency of the raw signal (in the present case study, the sampling frequency f_{s} was chosen as 20.48 MHz). The predicted locations of delamination are shown in table 3. Among the results, the maximum prediction error is 1.52%.

By increasing and decreasing the distance between the delamination and the right beam end, L, to 180 and 50 mm, respectively, while maintaining the delamination size and interlaminar position ($a = 25$ mm, between first and second laminae), the results accordingly processed are displayed in figures 6(a) and (b), respectively, while identification of the delamination location is detailed in table 4. As observed, there are normally several wave peaks following the incident Lamb wave (the first wave peak in the processed signal), which may make it difficult to recognize matching peaks reflected by the delamination. In particular for the case in figure 6(a), where

Table 3. Prediction results for selected samples.

Delaminated sample	Delamination parameters				Identification results	
	L (mm)	L' (mm)	a (mm)	Interlaminar position	L' (mm) (abs. error (%))	a (mm) (abs. error (%))
I	50	225	25	1–2	222.9 (0.93)	25.1 (0.4)
II	80	195	25	3–4	194.1 (0.46)	21.9 (12.4)
III	80	200	20	1–2	199.0 (0.5)	20.0 (0.0)
IV	80	185	35	1-2	184.5 (0.27)	34.4 (1.7)

Table 4. Prediction results for different delamination parameters.

	Delamination parameters			Identification results	
	L' (mm)	a (mm)	Interlaminar position	L' (mm) (abs. error (%))	a (mm) (abs. error (%))
Different delamination position	175	25	1–2	174.9 (0.06)	22.2 (11.2)
	155	25	1–2	155.8 (0.52)	22.1 (11.6)
	135	25	1–2	133.4 (0.44)	21.9 (12.4)
	225	25	1–2	222.9 (0.09)	25.1 (0.4)
	125	25	1–2	126.9 (1.52)	22.1 (11.6)
	95	25	1–2	95.3 (0.32)	22.1 (11.6)
Different delamination layer	195	25	2–3	194.1 (0.46)	22.1 (11.6)
	195	25	3–4	194.1 (0.46)	21.9 (12.4)
	195	25	4–5	194.1 (0.46)	21.9 (12.4)
	195	25	7–8	194.1 (0.46)	22.1 (11.6)
Different delamination size	200	20	1–2	199.0 (0.5)	20.0 (0.0)
	190	30	1–2	189.3 (0.37)	26.9 (10.3)
	185	35	1–2	184.5 (0.27)	34.4 (1.7)
	180	40	1–2	179.7 (0.17)	36.4 (9.0)

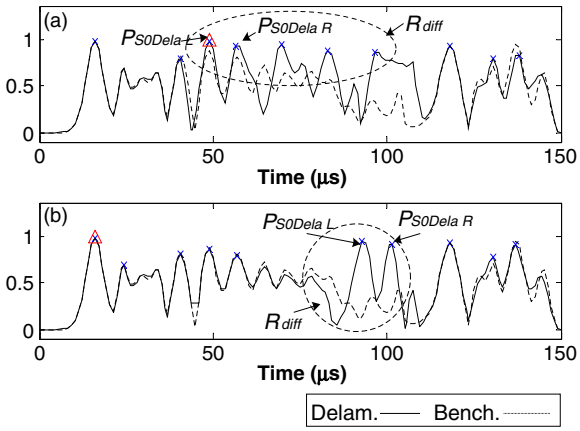

Figure 6. Envelope curves of CF-MP-processed Lamb wave signals from delaminated beams (a) $a = 25$ mm, $L = 180$ mm, $L' = 95$ mm, between the first and second layers; and (b) $a = 25$ mm, $L = 50$ mm, $L' = 225$ mm, between the first and second layers.

the delamination is very close to the right beam end, the waves reflected by the right delamination tip and the right beam end will overlap. Considering the current beam geometric features and Lamb wave propagation velocities, the explicit detectable range for the delamination is $L' \geqslant 95$ mm and $L \geqslant 30$ mm.

By changing the interlaminar position of the delamination while maintaining the delamination location and size, some new damage cases were evaluated, and the identification results using CF-MP approach are compared in table 4. The results show that the precision of prediction is not essentially dependent on the interlaminar position of the delamination. This observation suggests that Lamb waves might not be very sensitive to changes in the interlaminar position of delamination. However, this issue is less significant in practice, since damage due to low-velocity impact is normally manifested as a series of delaminations through the thickness of composite laminate rather than between two single layers only.

4.2. Delamination size

The key for quantifying delamination size is exact determination of the Lamb wave components reflected from the left and right delamination tips. Applying DWT-based digital filters, the signal component in the active excitation frequency range (0.1 MHz) was extracted and is displayed in figure 7(a). Without the interference of noise, the first wave packet is recognized as the incident S_0 first sensed by the sensor, and the last wave packet is the reflected wave from the right beam end, $S_{0\mathrm{ref}}$, between which is located the delamination-scattered Lamb wave, $S_{0\mathrm{Dela}}$, provided that the delamination is sufficiently large that reflection from the left and right delamination tips, $S_{0\mathrm{Dela\ L}}$ and $S_{0\mathrm{Dela\ R}}$ respectively, does not overlap in the time domain (the case for a small sample is discussed later), as shown in figure 7(b). Applying the CF-MP algorithm, the envelope curve of the signal was obtained (see figure 7(c)), from which the sampling points of interest were determined as

$$t_{\mathrm{S0}} = 501, \quad t_{\mathrm{S0Dela\ L}} = 1601, \quad \text{and} \quad t_{\mathrm{S0Dela\ R}} = 1701$$

where t_{S0}, $t_{\mathrm{S0Dela\ L}}$ and $t_{\mathrm{S0Dela\ R}}$ are the starting positions of the incident Lamb wave and reflected waves from left and right tips

Table 5. Characteristic data of reflected Lamb wave signal from delamination determined by the CF-MP approach.

Wave component	Position (sampling point) identified value (actual value)	Position (time (ms)) identified value (actual value)	K_τ
S_0	501 (501)	0.244 (0.244)	0.995 21
S_{0ref}	3301 (3301)	1.611 (1.611)	0.995 21
$S_{0Dela\ L}$	1601 (1601)	0.781 (0.781)	0.995 21
$S_{0Dela\ R}$	1701 (1701)	0.830 (0.830)	0.995 20

Table 6. Characteristic data of reflected Lamb wave signal from delamination with different levels of overlap.

Level of overlap	Position (sampling point) identified/actual/Abs. error (%)	Position (time (ms)) Identified/actual/Abs. error (%)	K_τ
42%	501/501/0	0.244/0.244/0.0	0.995 17
	3259/3259/0	1.591/1.591/0.0	0.995 20
	1601/1601/0	0.781/0.781/0.0	0.834 65
	1659/1659/0	0.810/0.810/0.0	0.861 01
55%	501/501/0	0.244/0.244/0.0	0.995 22
	3246/3246/0	1.584/1.584/0.0	0.995 22
	1602/1601/1	0.782/0.781/0.001	0.806 75
	1635/1646/11	0.798/0.803/0.005	0.780 58

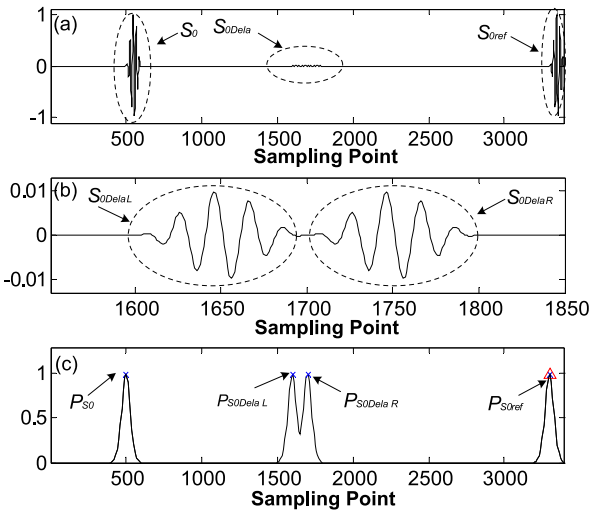

Figure 7. Delamination size assessment using correlation filtering: (a) DWT-filtered signal in the active excitation frequency range (0.1 MHz); (b) Lamb wave components reflected by the left and right tip of the delamination; (c) matching results upon application of CF-MP.

of the delamination in the envelope curve, respectively. The matching results and correlation coefficient, K, for the signal are given in table 5, from which the ToF between any two wave peaks can be calculated, and the length of the delamination can be determined with the known wave propagation velocity of the S_0 mode, V_{S0}, by (referring to figure 4)

$$a = \frac{(t_{S0Dela\ R} - t_{S0Dela\ L}) \cdot V_{S0}}{2 \cdot f_s}. \tag{12}$$

Prediction results for delamination size are also shown in table 4 for different composite beams with different delamination parameters, where the maximum error is 3.6 mm, about half the duration of the sinusoidal wave cycle.

When the delamination is not sufficiently large, the wave components reflected by its two tips can overlap even when CF-MP processing is applied, potentially resulting in poor identification precision. To evaluate the sensitivity of the approach, smaller delaminations were considered, including two cases of considerable overlap between left and right tip-reflected waves, 42% and 55% respectively, as shown in figures 8(a) and (b). For convenience of discussion, a parameter, D, was created to define the overlap degree by

$$D = \begin{cases} \dfrac{t_{S0Dela\ L} + T - t_{S0Dela\ R}}{T} \times 100\%, \\ \qquad \text{when } t_{S0Dela\ L} + T > t_{S0Dela\ R} \\ 0, \quad \text{else} \end{cases} \tag{13}$$

where T is the duration of the aforementioned incident wave, and the non-overlap degree, ξ, is $\xi = 1 - D$. The signals are not explicit enough to distinguish the waves reflected from the two delamination tips directly. Additionally, to further complicate the signal, random white noise was added into the signals. For convenience of discussion, a ratio, Σ, defined as the maximum peak–peak amplitude of the delamination-induced Lamb wave to the maximum peak–peak amplitude of noise, was introduced to define the noise level in the signal. As typical results, the envelope curves for the signals shown in figures 8(a) and (b) but with added white noise of $\Sigma = 0.5$, obtained using CF-MP processing, are exhibited in figures 8(c) and (d), respectively, where the first and last wave packets are the incident S_0 and its reflection from the right beam end. The identification results for delamination size are compared in table 6. The results indicate that the CF-MP-based signal processing approach is still able to deliver a satisfactory assessment when the overlap of reflection from both tips of delamination reaches 42%. It is also observed that, in the case of 55% overlap, CF-MP-based identification may produce a relatively large error. The minimum detectable size for a delamination, a_{min}, using a CF-MP-based process, can be

Table 7. Characteristic data of Lamb wave signal with different degrees of noise.

	Position (sampling point) identified value (actual value)	Position (time (ms)) identified value (actual value)	K_τ
Benchmark	501 (501)	0.244 (0.244)	0.995 11
	3301 (3301)	1.611 (1.611)	0.995 17
Delaminated $\Sigma = 2$	501 (501)	0.781 (0.781)	0.995 16
	3301 (3301)	0.244 (0.244)	0.995 20
	1601 (1601)	0.781 (0.781)	0.938 68
	1701 (1701)	0.830 (0.830)	0.934 63
Delaminated $\Sigma = 1$	501 (501)	0.244 (0.244)	0.995 11
	3301 (3301)	1.611 (1.611)	0.995 17
	1591 (1601)	0.776 (0.781)	0.828 32
	1701 (1701)	0.830 (0.830)	0.796 49
Delaminated $\Sigma = 0.5$	501 (501)	0.244 (0.244)	0.994 97
	3301 (3301)	1.611 (1.611)	0.995 10
	1591 (1601)	0.776 (0.781)	0.641 28
	1701 (1701)	0.830 (0.830)	0.527 20

approximated as (referring to figure 4)

$$a_{\min} = N \cdot \mathrm{int}\left(\frac{f_s}{f}\right) \cdot \xi_{\min} \cdot \left(\frac{1}{2} \times \frac{V_{S0}}{f_s}\right) \qquad (14)$$

where int(x) is the integral function, and N, f, f_s, and V_{S0} are the cycle number and central frequency of the excitation signal, sampling frequency, and propagation velocity of S_0 respectively; $\xi_{\min}$ denotes the detectable minimum non-overlap degree. Note that the fraction $\frac{1}{2}$ is for the present case where the sensor is located between the actuator and the damage. When a 2.48 MHz sampling rate is used, equation (14) goes to 8 mm.

4.3. Noise tolerance

In practice, captured Lamb wave signals are prone to contamination from a diversity of noise sources, including random ambient electrical/magnetic interference, background sinusoidal signal and structural low-frequency vibration. All of these can hamper the correct understanding of a Lamb wave signal.

To examine the tolerance of the CF-MP approach to noise, artificial noise was added into the simulated Lamb wave signals. Considering the example discussed in section 4.1, the Lamb wave signal captured from a delamination-free composite beam is shown in figure 9(a), serving as a benchmark signal. Random white noise was added into the raw signal (around 1% of the maximum peak–peak amplitude of the incident energy). The envelope curve of the signal, obtained using CF-MP, is displayed in figure 9(b). In the case of a delamination occurring (referring to table 7 for delamination parameters) and random white noise with $\Sigma = 1$ added, the captured Lamb wave signal is shown in figure 9(c), with a magnified segment in figure 9(d). Exacerbated by the noise, the signal cannot be explicitly interpreted. Upon application of CF-MP, the Lamb waves reflected from both tips of the delamination are clearly present in the processed results, figure 9(e), where the dotted line is the benchmark signal for comparison. Repeating the above examination by adding more noise ($\Sigma = 0.5$) and less noise ($\Sigma = 2$), the raw Lamb wave signals obtained as well as the CF-MP-processed results when $\Sigma = 0.5$, as an example, are compared in figures 9(f)–(h). In the processed result, two wave components reflected from both tips of the delamination can be clearly observed, contributing to exact assessment of the delamination location, as detailed in table 7.

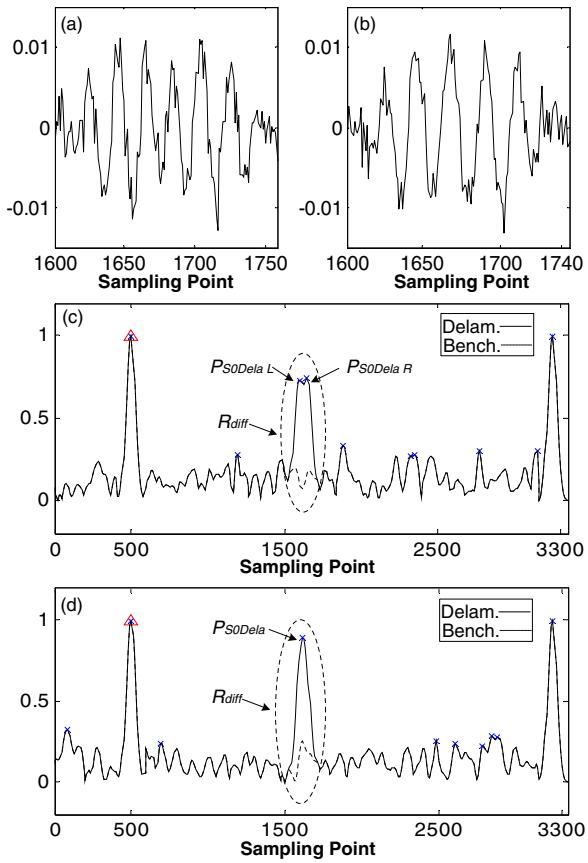

Figure 8. Overlapped Lamb waves reflected from the delamination; (a) 42% overlap; (b) 55% overlap; (c) CF-MP-processed envelope curve of (a); (d) CF-MP-processed envelope curve of (b).

Both figure 9 and table 7 have demonstrated that the CF-MP approach is able to offer explicit signal interpretation even when the background noise is very strong, and the prediction

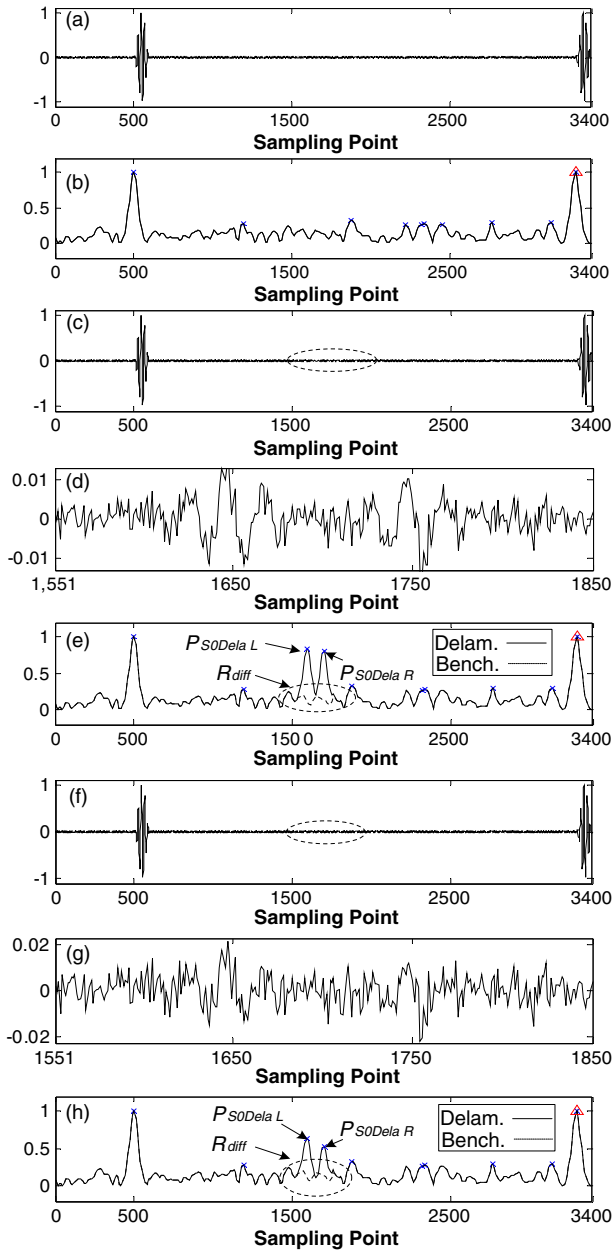

Figure 9. Delamination identification from Lamb wave signals with noise: (a) raw signal without delamination; (b) CF-MP-processed results of (a); (c) raw signal with delamination and $\Sigma = 1$; (d) magnified part of (c); (e) CF-MP-processed results of (c); (f) raw signal with delamination and $\Sigma = 0.5$; (g) magnified part of (f); and (h) CF-MP-processing results of (f).

error for the delamination size, $\Delta L'$, can be calculated:

$$\Delta L' = \left(\frac{1}{2} \times \frac{1}{f}\right) \cdot V_{S0} = \left(\frac{1}{2} \times \frac{1}{0.5}\right) \cdot 5800 \approx 3 \text{ mm} \quad (15)$$

where f is the excitation frequency of 0.5 MHz and V_{S0} is around 5800 m s^{-1} for the current material properties and laminate thickness.

A slight deviation of the reflected signals from both tips of the delamination and the structural boundary is normally observed in the signals [8], leading to a slight bias in phase and amplitude, and the current study is no exception. Such a phenomenon can be attributed to the unique attenuation mechanism of Lamb waves in elastic materials. However, it is noteworthy that the decrease in the reflected amplitude from the delamination would not reduce the effectiveness of CF-MP-based identification, since the correlation coefficient K_τ is a normalized parameter.

5. Conclusion

A correlation filtering-based matching pursuit (CF-MP) signal processing approach was developed in this study, aimed at exactly evaluating the location and size of structural damage by interpreting captured Lamb wave signals. This approach was used to evaluate Lamb wave signals in different delamination cases of CF/EP composite beams. The results demonstrate that CF-MP-based signal processing is able to quantitatively identify both the location and size of delamination in the composite beams from Lamb wave signals, even in cases where the delamination is small and background noise is high.

Acknowledgments

F Li and G Meng are grateful for the support received from the Natural Science Foundation of China (NSFC No 50575146), NSFC Joint Research Fund for Overseas Chinese Young Scholars (No 10528206) and Key International S&T Cooperation Project of China Ministry of Science and Technology (No 2005DFA00110), respectively. Z Su and L Ye are grateful for research project grants of an Australian Postdoctoral Fellowship (APF) and Discovery Project (DP) from the Australian Research Council, respectively.

References

[1] Guo N and Cawley P 1992 Lamb waves for the NDE of composite laminates *Review of Progress in Quantitative Nondestructive Evaluation* ed D O Thompson and D E Chimenti (New York: Plenum) pp 1443–50

[2] Lin X and Yuan F G 2001 Diagnostic Lamb waves in an integrated piezoelectric sensor/actuator plate: analytical and experimental studies *Smart Mater. Struct.* **10** 907–13

[3] Badcock R A and Birt E A 2000 The use of 0-3 piezocomposite embedded Lamb wave sensors for detection of damage in advanced fibre composites *Smart Mater. Struct.* **9** 291–7

[4] Kessler S S, Spearing S M and Atalla M J 2002 In-situ damage detection of composites structures using Lamb wave methods *Proc. 1st European Workshop on Structural Health Monitoring (Paris, France)* ed D Balageas, pp 374–81

[5] Wang C S and Chang F-K 1999 Built-in diagnostics for impact damage identification of composite structures *Structural Health Monitoring* 2nd edn, ed F-K Chang (Lancaster: Technomic) pp 612–21

[6] Lemistre R G M, Kaczmarek H and Balageas D 1999 Damage localization in composite plates using wavelet transform processing on Lamb wave signals *Structural Health Monitoring* 2nd edn, ed F K Chang (Lancaster: Technomic) pp 861–70

[7] Alleyne D N and Cawley P 1992 The interaction of Lamb waves with defects *IEEE Trans. Ultrason. Ferroelectr. Freq. Control* **39** 381–97

[8] Kessler S S, Spearing S M and Soutis C 2002 Damage detection in composite materials using Lamb wave methods *Smart Mater. Struct.* **11** 269–78

[9] Sohn H and Farrar C R 2001 Damage diagnosis using time series analysis of vibration signals *Smart Mater. Struct.* **10** 446–51
[10] Keilers C H and Chang F K 1995 Identifying delamination in composite beams using built-in piezoelectrics, part I: experiments and analysis *J. Intell. Mater. Syst. Struct.* **6** 649–63
[11] Keilers C H 1998 Search strategies for identifying a composite plate delamination using built-in transducers *J. Intell. Mater. Syst. Struct.* **9** 883–91
[12] Kawiecki G 1998 Feasibility of applying distributed piezotransducers to structural damage detection *J. Intell. Mater. Syst. Struct.* **9** 189–97
[13] Blanas P, Rigas E and Das-Gupta D K 1999 Health monitoring of composite structures using composite piezoelectric transducers *Structural Health Monitoring* 2nd edn, ed F K Chang (Lancaster: Technomic) pp 635–42
[14] Kim Y Y and Kim E H 2001 Effectiveness of the continuous wavelet transform in the analysis of some dispersive elastic waves *J. Acoust. Soc. Am.* **110** 86–94
[15] Li C J and Ma J 1997 Wavelet decomposition of vibrations for defection of bearing-localized defects *NDT & E Int.* **30** 143–9
[16] Wang W J and McFadden P D 1993 Early detection of gear failure by vibration analysis, part I: calculation of the time-frequency distribution *Mech. Syst. Signal Process.* **7** 193–203
[17] Legendre S, Massicotte D, Goyette J and Bose T K 2000 Wavelet-transform-based method of analysis for Lamb-wave ultrasonic NDE signals *IEEE Trans. Instrum. Meas.* **49** 524–30
[18] Daubechies I 1990 The wavelet transform, time-frequency localization and signal analysis *IEEE Trans. Inform. Theory* **36** 961–1005
[19] Okafor A C and Dutta A 2000 Structural damage detection in beams by wavelet transforms *Smart Mater. Struct.* **9** 906–17
[20] Sung D-U, Oh J-H, Kim C-G and Hong C-S 2000 Impact monitoring of smart composite laminates using neural network and wavelet analysis *J. Intell. Mater. Syst. Struct.* **11** 180–90
[21] Yam L H, Yan Y J and Jiang J S 2003 Vibration-based damage detection for composite structures using wavelet transform and neural network identification *Compos. Struct.* **60** 403–12
[22] Valdes S H D and Soutis C 2001 A structural health monitoring system for laminated composites *Proc. DETC (Pittsburgh, PA)* pp 2013–21
[23] Hou J, Leonard K R and Hinders M K 2004 Automatic multi-mode Lamb wave arrival time extraction for improved tomographic reconstruction *Inverse Problems* **20** 1873–88
[24] Mallat S G and Zhang Z F 1993 Matching pursuits with time-frequency dictionaries *IEEE Trans. Signal Process.* **41** 3397–415
[25] Vera-Candeas P, Ruiz-Reyes N, Rosa-Zurera M, Martinez-Munoz D and Lopez-Ferreras F 2004 Transient modeling by matching pursuits with a wavelet dictionary for parametric audio coding *IEEE Signal Process. Lett.* **11** 349–52
[26] Daubechies I 1992 *Ten Lectures on Wavelets* (Philadelphia, PA: Society for Industrial and Applied Mathematics)
[27] Mathworks Inc. 2000 *Wavelet Toolbox: For Use with Matlab (User's Guide) Version 1.0* (Sherborn, MA: Mahtworks Inc.)
[28] Freudinger L C, Lind R and Brenner M J 1998 Correlation filtering of modal dynamics using the Laplace wavelet *Proc. 16th Int. Modal Analysis Conf. (Santa Barbara, CA, Feb. 1998)* pp 868–77
[29] Zi Y 2000 *Research on Un-stationary Signal Feature Extraction Theory Based Diagnostic Technologies* (Xi'an: Xi'an Jiaotong University Publishing House)
[30] Su Z and Ye L 2005 Lamb wave propagation-based damage identification for quasi-isotropic CF/EP composite laminates using artificial neural algorithm, part I: methodology and database development *J. Intell. Mater. Syst. Struct.* **16** 97–111
[31] Su Z and Ye L 2005 Lamb wave propagation-based damage identification for quasi-isotropic CF/EP composite laminates using artificial neural algorithm, part II: implementation and validation *J. Intell. Mater. Syst. Struct.* **16** 113–25
[32] Su Z and Ye L 2002 A damage identification technique for CF/EP composite laminates using distributed piezoelectric transducers *Compos. Struct.* **57** 465–71